

# In-situ electrochemical X-ray diffraction: A rigorous method to navigate within phase diagrams reveals $\beta$ -Fe<sub>1+x</sub>Se as superconductor for all $x$

Bertold Rasche,<sup>1,\*</sup> Minjun Yang,<sup>1</sup> Lothar Nikonow,<sup>1</sup> Joshaniel F K Cooper,<sup>2</sup> Claire A Murray,<sup>3</sup> Sarah J Day,<sup>3</sup> Karin Kleiner,<sup>3</sup> Simon J Clarke,<sup>1,†</sup> and Richard G Compton<sup>1,‡</sup>

<sup>1</sup>*Department of Chemistry, University of Oxford,  
Oxford, OX1 3QZ, United Kingdom*

<sup>2</sup>*ISIS Neutron and Muon Source, Rutherford Appleton Laboratory,  
Harwell Campus, Didcot OX11 0QX, United Kingdom*

<sup>3</sup>*Diamond Light Source, Harwell Campus,  
Didcot OX11 0QX, United Kingdom*

(Dated: August 19, 2019)

## Abstract

We report the precise postsynthetic control of the composition of  $\beta$ -Fe<sub>1+x</sub>Se by electrochemistry with simultaneous tracking of the associated structural changes via in-situ synchrotron X-ray diffraction. We access the full phase width of  $0.01 < x < 0.04$  and identify the superconducting state below 8 K, which in contrast to earlier reports is independent of the composition. However, in a second set of in-situ X-ray diffraction experiments, we demonstrate that  $\beta$ -Fe<sub>1+x</sub>Se forms a new phase in the presence of oxygen above a 100 °C which has the same anti-PbO type structure but is not superconducting down to 1.8 K. The latter process can be reversed electrochemically to reinstate the superconducting state. These observations exploit the exquisite control afforded by electrochemistry in contrast with classical approaches of chemical synthesis.

---

\* bertold.rasche@chem.ox.ac.uk

† simon.clarke@chem.ox.ac.uk

‡ richard.compton@chem.ox.ac.uk

One of the remaining challenges in the big riddle of the superconducting state is that of the iron-based superconductors. While the iron atom is associated with magnetism the superconducting state is based on the seemingly antagonistic Cooper pairs.[1–3] Understanding of this materials family is growing and it seems that for most structures with a superconducting phase there exists a so-called parent phase with an anti-ferromagnetic ground state, normally a stoichiometric phase with Fe in the +2 state.[4–6] It is however extraordinary how the smallest changes in composition and structure can lead to a changed ground state. This is already known for the first class of high-temperature superconductors, the cuprates, with their sensitivity towards oxygen defects [7, 8] and is true for one of the “simplest” iron-based superconductors:  $\beta$ -Fe<sub>1+x</sub>Se.

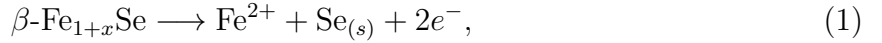
The difficulty of understanding the superconducting state in the “simple” tetragonal structure of  $\beta$ -Fe<sub>1+x</sub>Se arises from its narrow phase width ( $0.01 < x < 0.04$ ), a small deviation from the 1:1-ratio and its manifold of neighbouring phases (Figure 1).[9, 10] Its superconductivity[11] has been reported to be heavily dependent on the composition[12] and closely related structural transitions and various superstructures. Most prominently, the existence of the tetragonal-to-orthorhombic transition at around 80 K was found to be critical for  $\beta$ -Fe<sub>1+x</sub>Se to become superconducting at temperatures around 8 K.[13, 14] If this transition is not observed, one finds a tetragonal-to-triclinic transition at 60 K and no superconducting state down to 2.0 K.[15, 16] The only difference that leads to this changed behaviour is that the latter samples were grown hydrothermally, while the superconducting samples resulted from a classic solid-state synthesis. Recently, samples grown by vapour transport showed no indication of a composition dependence of the superconducting transition temperature, but rather, showed that disorder, as quantified by the residual resistivity ratio, was the crucial factor.[17] Finally, the confusion becomes perfect, with the inclusion of samples grown via molecular beam epitaxy (MBE), which were found to exhibit certain superstructures only observable in electron diffraction, that also rendered the  $\beta$ -Fe<sub>1+x</sub>Se structure non-superconducting within the measured temperature window.[18] On the other hand, MBE samples grown on a SrTiO<sub>3</sub> substrate already became superconducting at 100 K.[19]

This sensitivity towards composition and related structural effects dictates an approach in which structural and compositional changes are rigorously correlated. In this respect, methods like MBE growth have to be taken with care, as they keep the kinetic activation to a minimum and therefore extend the phase diagram towards metastable and strained phases. If one therefore focuses on thermodynamically stable products it becomes necessary to change the parameters defining the thermodynamic ground state while tracing the structure. This has been achieved for iron-based superconductors in in-situ experiments by changing the temperature[13, 14, 20], pressure[21–24] and to some extent the composition, the latter via initiating a chemical reaction to tune the electron count at very low temperatures using intercalation.[25, 26] In contrast, we focus on one very direct influence on any redox reaction, the electrochemical potential. And while chalcogenides have been investigated electrochemically for a long time,[27–29] with respect to structure-property relationships of superconductors, the electrochemical potential as parameter has only been exploited for intercalation reactions,[30, 31] as they are well known and extensively studied in (lithium) battery research.[32–35] But focussing on intercalation reactions confines this powerful method, as we demonstrate.

We have performed experiments with  $\beta\text{-Fe}_{1+x}\text{Se}$  immobilised onto an electrode in an electrochemical in-situ X-ray diffraction (XRD) cell with oxygen free, aqueous solutions as electrolyte (details see SI Methods). In a three electrode set-up with a reference and a counter electrode, the potential was slowly changed by scanning at a rate of  $0.001\text{ Vs}^{-1}$ , the current was measured and the structural changes were traced via continuously recording XRD patterns (details see SI Methods). At key stages during the scans, samples were extracted for magnetisation measurements to determine the superconducting transition temperature. Finally, we compared this method of changing the thermodynamic ground state to a complementary approach via changing the temperature and investigated the influence of oxygen to follow in-situ the structural transition that renders  $\beta\text{-Fe}_{1+x}\text{Se}$  non-superconducting.

### *Electrochemical experiments*

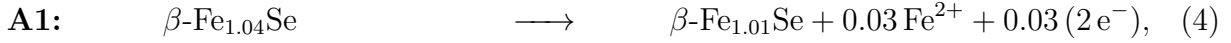
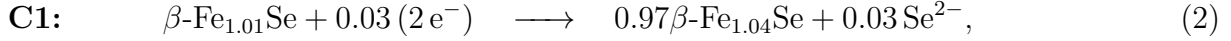
A citrate buffer (0.1 M) with  $pH=7$  and KCl (0.1 M) as supporting electrolyte at  $65\text{ }^{\circ}\text{C}$  was identified as suitable working conditions (SI Section II.A). With the  $\beta\text{-Fe}_{1+x}\text{Se}$  immobilised on the working electrode (SI Methods), the potential was scanned from the approximate open circuit potential of  $-0.8\text{ V}$  vs. SCE, first reductively to  $-1.25\text{ V}$  and then oxidatively to  $+0.75\text{ V}$ . The current reveals one small signal on reduction (Figure 2a and c: **C1**) at ca.  $-1.2\text{ V}$ , two small signals (Figure 2a and c: **A<sub>Fe</sub>**, **A1**) and one dominant signal with a double peak (Figure 2a: **A2**) on oxidation at ca.  $-0.9\text{ V}$ ,  $-0.6\text{ V}$  and  $0.0\text{ V}$ , respectively. The diffraction patterns reveal that the latter signal at  $0.0\text{ V}$  can be assigned to the complete oxidation of  $\beta\text{-Fe}_{1+x}\text{Se}$  according to:



as the diffraction peaks of  $\beta\text{-Fe}_{1+x}\text{Se}$  vanish and new diffraction peaks appear which can be indexed as trigonal selenium (Figure 2b, SI: Figure S.10 and gif online). The increasing noise during the oxidation and the observed double peak is attributed to the formed semi-conducting selenium introducing an increasing resistance, as known from selenium deposition.[36]

By taking a closer look at the potential range between  $-1.25\text{ V}$  and  $-0.5\text{ V}$  in which the structure of  $\beta\text{-Fe}_{1+x}\text{Se}$  remains intact (Figure 2c), it becomes obvious that the signals **C1** and **A1** are related to subtle but significant changes of the structure. Considering the phase diagram (Figure 1) one can expect a reduction/oxidation with a small signal compared to the full oxidation (reaction (1)) due to the reported phase width. We therefore refined the Fe/Se-ratio in the structure of  $\beta\text{-Fe}_{1+x}\text{Se}$  which rises with the reductive signal **C1** at  $-1.2\text{ V}$  and decreases with the oxidative signal **A1** at  $-0.6\text{ V}$  (Figure 2c). Using the  $c/a$ -ratio as an indicator for the Fe/Se-ratio,[12, 23] which is less prone to any refinement issues as it only relies on the diffraction peak positions (not the integral intensity), this structural change becomes even more pronounced (Figure 2c). Our in-situ experiments thereby also validate the  $c/a$ -ratio as a reliable parameter for the Fe/Se-ratio (see also SI: Figure S.2).

In accordance with the Fe-Se phase diagram (Figure 1b) we assign the following processes:



The reason these equations can be written in two different ways relates to the fact that in  $\beta\text{-Fe}_{1+x}\text{Se}$  the occupancy of the Fe-sites and the Se-site are correlated, so *a priori* one cannot differentiate between a change of the occupancy of the Se-site (eq. (3) and (5)) or a change of the occupancy of the Fe-sites (eq. (2) and (4)). Furthermore, both descriptions, either with selenium vacancies or with iron on an interstitial (octahedral) position, are feasible.[10, 12, 37, 38] As we find that refinement of the octahedral site yields no significant occupancy at any stage we decided to plot the Fe/Se-ratio. Furthermore, due to the low expected deviation from the Fe:Se = 1:1-ratio (in electrons:  $0.04 * 26e^- (n_{e^-}(\text{Fe})) = 1.04e^-$ ) and the fact that we abstained from using a diffraction standard for the electrochemical experiment due to possible interferences, the Rietveld refinement is also prone to a systematic error concerning the Fe/Se-ratio. In our case this yields a Fe/Se-ratio of 0.96:1 versus a Fe/Se-ratio of 1.01:1 from the composition used in the synthesis. The latter agrees with the Fe/Se-ratio from a separate synchrotron XRD experiment *with* a diffraction standard (SI: Figure S.1 and S.2). Therefore, as in the in-situ experiment we directly track the structural changes independent of a systematic error, we decided to plot the *change* of the Fe/Se-ratio where no diffraction standard was used and only use the Fe/Se-ratio itself where such a standard was used.

Whether one assumes selenium vacancies or iron interstitials, it is important to notice that eq. (3) or (2) are different chemical reactions than eq. (5) or (4), as the first involve Se-ions and the latter Fe-ions. In separate experiments, we could confirm the reversibility of reaction (5)/(4) with  $\text{Fe}^{2+}$  in solution, where we stopped the oxidation after signal **A1** and reversed the scan direction scanning back to  $-1.0\text{ V}$ . These experiments are discussed in the

## SI Section II.E.

Apart from the structural changes in this partial oxidation/reduction one also observes that during the complete oxidation **A2** the  $c/a$ -ratio increases again (Figure 2a). We speculate this might be related to the decomposition mechanism of  $\beta\text{-Fe}_{1+x}\text{Se}$  in which the interlayer space increases to enable diffusion of the iron ions while solid selenium is forming.

Concerning the phase width of  $\beta\text{-Fe}_{1+x}\text{Se}$  we get  $\Delta x = 0.009$  and  $\Delta x = 0.025$  from integration of the current peaks **C1** and **A1**, respectively and comparing it to the charge of the complete oxidation **A2**. The value from the oxidation **A1** is in accordance with the reported phase width of 0.03 and the change of the Fe/Se-ratio from Rietveld refinement of 0.04 (see also Figure 3b). The lower value for **C1** could hint towards a sample that was initially not fully oxidised, although the used composition  $\text{Fe}_{1.01}\text{Se}$  is considered the most oxidised composition. On the other hand, the reduction process (3) is overlaid with the onset of the hydrogen evolution reaction (HER), which complicates integration.

Finally, we assign the small signal **A<sub>Fe</sub>** on oxidation at  $-0.9\text{ V}$  to the oxidation of traces of elemental iron to  $\text{Fe}^{2+}$  in solution. The assignment follows separate experiments with iron and  $\text{Fe}^{2+}$  solutions (SI Section II.B) and the fact that traces of elemental iron ( $\approx 0.5\%$  from Rietveld refinement) were found in the starting sample. From charge integration these impurities amount to  $0.1\%$  compared to charge for the full oxidation of  $\text{Fe}_{1+x}\text{Se}$  (**A2**), demonstrating the sensitivity of the electrochemical approach.

Having established a method to change the composition “vertically” (isothermally) at relatively low temperatures, we investigated the superconducting properties of the  $\beta\text{-Fe}_{1+x}\text{Se}$  samples within the phase width, as a high sensitivity of the superconducting transition temperature was reported.[12] We therefore considered representative samples at different stages of the electrochemical experiment and measured their magnetisation (Figure 3c). We chose a  $\beta\text{-Fe}_{1.01}\text{Se}$  sample from synthesis, a sample after the reduction **C1** (black square Figure 2a and c), a sample after oxidation **A1** (red square Figure 2a and c), a sample halfway into the full oxidation of  $\beta\text{-Fe}_{1+x}\text{Se}$  **A2** (turquoise square Figure 2a) and a sample which after oxidation **A1** was reduced in a  $0.1\text{ M Fe}^{2+}$  solution (SI Section II.E). The  $c/a$ -

ratio and the Fe/Se-ratio were determined using a lab diffractometer (SI Figure S.11). As explained above we use  $\Delta(c/a)$  and  $\Delta(\text{Fe/Se})$  to compare the in-situ synchrotron XRD experiments and the lab diffractometer results. While the structural parameters agree with the expectations for a sample being reduced ( $\beta\text{-Fe}_{1.04}\text{Se}$ ), oxidised ( $\beta\text{-Fe}_{1.01}\text{Se}$ ) or at halfway to full oxidation (Figure 3b), the magnetisation measurements reveal the same sharp  $T_c$  at ca. 8 K for *all* samples (Figure 3c). For the sample halfway into the full oxidation the slope of the magnetic susceptibility  $\chi$  is smaller, in agreement with the fact that a substantial part of the material will have been transformed into selenium. We point out, that the superconducting volume fraction is slightly lower than in other literature reports,[12, 16] due to the fact that our samples have a very isotropic morphology due to the powder synthesis, grinding and sieving, and were measured at fields roughly ten times as high. A detailed discussion of these influences can be found in the SI Section I.G.

Our finding that the composition within the phase width of  $\beta\text{-Fe}_{1+x}\text{Se}$  has no influence on the onset temperature of the superconductivity is in line with a report that the transition temperature varies between samples with similar compositions, but different levels of disorder quantified by the residual resistivity ratio.[17] But there are several reports which find that the  $\beta\text{-Fe}_{1+x}\text{Se}$  structure shows no superconductivity down to 2 K.[12, 15, 16] Therefore, we considered initial hints of another phase transition which might be responsible for  $\beta\text{-Fe}_{1+x}\text{Se}$  becoming non-superconducting.[12]

### *Heating experiments*

To investigate this further, pre-synthesised samples of  $\beta\text{-Fe}_{1+x}\text{Se}$  were prepared in 0.3 mm silica capillaries of which one was sealed under argon, one was sealed after exposing it to air and therefore containing a fixed amount of oxygen, and one was left open. These samples were heated from 25 °C to 200 °C while measuring XRD patterns in-situ. Figure 3a demonstrates how the  $c/a$ -ratio and simultaneously the Fe/Se-ratio change significantly above 100 °C. Under argon, this change is reversible and only observable in the  $c/a$ -ratio (not in

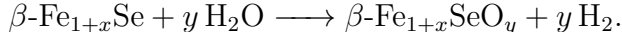
the Fe/Se-ratio), with the structure remaining intact. We do not find evidence for any decomposition of  $\beta\text{-Fe}_{1+x}\text{Se}$  at the temperatures studied as reported by McQueen *et al.*[12]. Nevertheless, in case of the oxygen containing samples the change is much more pronounced. For the oxygen exposed samples there is a distinct step in the Fe/Se-ratio between 100 °C and 150 °C concomitant with the deviation from the  $c/a$ -curve of the argon sample. After this step, the Fe/Se-ratio of the sample with a limited amount of oxygen remains relatively constant and the trend of the  $c/a$ -curve follows the trend of the sample under argon (shifted only by a fixed value). The sample exposed to air however starts to decompose above 150 °C, which involves an even stronger decrease in both the Fe/Se-ratio and the  $c/a$ -ratio. For this sample, eventually  $\text{Fe}_3\text{Se}_4$  can be indexed in the diffraction pattern (SI Figure S.14), which is the next neighbouring Se-richer phase of  $\beta\text{-Fe}_{1+x}\text{Se}$  in the phase diagram (Figure 1).

For the sample under argon and the partially oxidised sample a diffraction pattern was taken at 80 K (before and after heating to 200 °C), to check for the reported tetragonal-to-orthorhombic phase transition around 100 K (SI Figure S.12). Before heating, both samples were best refined with an orthorhombic cell at 80 K, while after the heating experiment only in case of the sample kept under argon this was true and the partially oxidised sample did not show any phase transition and was best refined with the tetragonal cell. Accordingly, the measured magnetisation shows superconducting behaviour below 8 K in the case of the sample kept under argon both before and after the heating, while the partially oxidised sample loses its superconducting properties after being heated (Figure 3c).

This observation allows us to conclude that above 100 °C  $\beta\text{-Fe}_{1+x}\text{Se}$  can undergo a phase transition when exposed to air, that is not related to the phase width of the structure. We cannot find indication of any other phases being formed during this process as long as the complete oxidation is avoided by either limiting the oxygen amount or by not heating above 150 °C. The uptake of oxygen during this phase transition is further examined with a thermogravimetric analysis (TGA, SI Section IV.B). In addition, no comparable irreversible phase transition is observed for  $\beta\text{-Fe}_{1+x}\text{Se}$  under argon. This implies that oxygen is incorporated into the structure rendering it  $\beta\text{-Fe}_{1+x}\text{SeO}_y$ , which agrees with EELS measurements



that first indicated the existence of such a phase.[12] From the TGA we calculate  $y = 0.002$ . In general, this result cannot only explain the reported “oxygen poisoning”[12] but also why hydrothermally synthesised samples are non-superconducting.[15, 16] For the latter, we speculate that the oxygen is provided by a redox reaction above 100 °C of  $\beta$ -Fe<sub>1+x</sub>Se and H<sub>2</sub>O in which very small amounts of H<sub>2</sub> are formed, according to:



In addition, the reported dependency of the superconducting transition temperature on disorder could help to understand how such small amounts of oxygen can change the superconducting behaviour.[17] The influence of the oxygen on the properties of the  $\beta$ -Fe<sub>1+x</sub>Se would then not be related to the chemical and/or electronic nature of the atoms, but rather on the disorder following from the incorporation of an impurity. We highlight that the changes in the lattice parameters are relatively small and only recognisable in an in-situ experiment where the lattice parameters are tracked continuously and the sample is fixed throughout, with the phase transition only clearly showing up in the more sensitive  $c/a$ -ratio (SI Figure S.12).

Finally, the strength of the introduced electrochemical approach can be used to recover the superconductivity for a sample oxidised in air  $\beta$ -Fe<sub>1+x</sub>SeO<sub>y</sub>. By preparing the oxidised sample on an electrode as discussed for the other  $\beta$ -Fe<sub>1+x</sub>Se samples, and scanning the potential down to  $-1.6 \text{ V}$  vs. SCE at  $-0.001 \text{ V s}^{-1}$  the superconducting behaviour was reinstated, although with a broadened transition and a slightly lower onset temperature (Figure 3c). The corresponding reduction process must occur between  $-1.25 \text{ V}$  and  $-1.6 \text{ V}$ , as for a sample extracted at  $-1.25 \text{ V}$  the superconductivity was not yet recovered. On the other hand, we cannot identify a distinct signal for this reduction process, because within the mentioned potential range the solvent starts to break down, which most likely masks the signal of the  $\beta$ -Fe<sub>1+x</sub>SeO<sub>y</sub> reduction. This could also explain the lower onset for the superconducting transition, as the reduction might have not been complete.

In summary, at 65 °C we were able to reversibly screen the very narrow phase width of

$\beta$ -Fe<sub>1+x</sub>Se electrochemically. Furthermore, on oxidation we can separate the related potential of this partial oxidation from the potential of the complete oxidation of  $\beta$ -Fe<sub>1+x</sub>Se to selenium and Fe<sup>2+</sup>. At each relevant stage during the electrochemical experiment a sample was taken and the superconducting transition temperature was measured. Thereby, we reveal that the phase width of  $\beta$ -Fe<sub>1+x</sub>Se has no influence on the superconducting properties, in contrast to earlier reports but in line with a recent investigation that reveals disorder as the main suppressor of the superconductivity.[12, 17]

Furthermore, upon heating to 200 °C in an oxygen containing atmosphere  $\beta$ -Fe<sub>1+x</sub>Se undergoes a phase transition in which a small amount of oxygen is incorporated into the structure rendering the sample non-superconducting down to 1.8 K. This process can be reversed using our electrochemical approach allowing us to recover the superconducting properties by electrochemical reduction of an air-oxidised sample. Our results offer a way to understand the long-standing puzzle that  $\beta$ -Fe<sub>1+x</sub>Se synthesised hydrothermally[16] or using aqueous methods[15] do not show superconductivity.

## ACKNOWLEDGEMENTS

We thank Dr. Simon Cassidy for his support concerning Rietveld refinements in TOPAS and Dr. Enno Kätelhön for support with the Python scripting. B.R. acknowledges the financial support from the German Research Foundation (DFG) through the Research Fellowship RA 3120/1-1. M.Y. acknowledges funding via the EPSRC Industrial CASE award EP/N509711/1. This work was carried out with the support of the Diamond Light Source, instrument I11 (proposal EE20638-1). The authors declare that they have no competing financial interests.

- 
- [1] D. C. Johnston, *Adv. Phys.* **2010**, *59*, 803–1061.
  - [2] J. Paglione, R. L. Greene, *Nat. Phys.* **2010**, *6*, 645–658.
  - [3] D. Johrendt, *J. Mater. Chem.* **2011**, *21*, 13726–13736.
  - [4] P. J. Hirschfeld, M. M. Korshunov, I. I. Mazin, *Rep. Prog. Phys.* **2011**, *74*, 124508.
  - [5] J. C. S. Davis, D.-H. Lee, *PNAS* **2013**, *110*, 17623–17630.
  - [6] Y. Gu, Z. Liu, T. Xie, W. Zhang, D. Gong, D. Hu, X. Ma, C. Li, L. Zhao, L. Lin, Z. Xu, G. Tan, G. Chen, Z. Y. Meng, Y.-f. Yang, H. Luo, S. Li, *Phys. Rev. Lett.* **2017**, *119*, 157001.
  - [7] Y. Suyama, M. Matsumoto, S. Kageyama, I. Sato, *Effect of Oxygen Deficiency on the Superconducting Properties of YBCO in Advances in Superconductivity III*, K. Kajimura, H. Hayakawa (Eds.), Springer Japan, Tokyo, **1991**, pp. 391–394.
  - [8] J. L. Tallon, *Oxygen in High-T<sub>c</sub> Cuprate Superconductors in Frontiers in Superconducting Materials*, A. V. Narlikar (Ed.), Springer-Verlag, Berlin/Heidelberg, **2005**, pp. 295–330.
  - [9] H. Okamoto, *JPE* **1991**, *12*, 383–389.
  - [10] A. J. Williams, T. M. McQueen, R. J. Cava, *Solid State Commun.* **2009**, *149*, 1507–1509.
  - [11] F.-C. Hsu, J.-Y. Luo, K.-W. Yeh, T.-K. Chen, T.-W. Huang, P. M. Wu, Y.-C. Lee, Y.-L. Huang, Y.-Y. Chu, D.-C. Yan, M.-K. Wu, *PNAS* **2008**, *105*, 14262–14264.
  - [12] T. M. McQueen, Q. Huang, V. Ksenofontov, C. Felser, Q. Xu, H. Zandbergen, Y. S. Hor, J. Allred, A. J. Williams, D. Qu, J. Checkelsky, N. P. Ong, R. J. Cava, *Phys. Rev. B* **2009**, *79*, 014522.
  - [13] S. Margadonna, Y. Takabayashi, M. T. McDonald, K. Kasperkiewicz, Y. Mizuguchi, Y. Takano, A. N. Fitch, E. Suard, K. Prassides, *Chem. Commun.* **2008**, *0*, 5607–5609.
  - [14] T. M. McQueen, A. J. Williams, P. W. Stephens, J. Tao, Y. Zhu, V. Ksenofontov, F. Casper, C. Felser, R. J. Cava, *Phys. Rev. Lett.* **2009**, *103*, 057002.
  - [15] F. Nitsche, T. Goltz, H.-H. Klauss, A. Isaeva, U. Müller, W. Schnelle, P. Simon, T. Doert, M. Ruck, *Inorg. Chem.* **2012**, *51*, 7370–7376.
  - [16] U. Pachmayr, N. Fehn, D. Johrendt, *Chem. Commun.* **2015**, *52*, 194–197.
  - [17] A. E. Böhmer, V. Taufour, W. E. Straszheim, T. Wolf, P. C. Canfield, *Phys. Rev. B* **2016**, *94*, 024526.

- [18] T.-K. Chen, C.-C. Chang, H.-H. Chang, A.-H. Fang, C.-H. Wang, W.-H. Chao, C.-M. Tseng, Y.-C. Lee, Y.-R. Wu, M.-H. Wen, H.-Y. Tang, F.-R. Chen, M.-J. Wang, M.-K. Wu, D. V. Dyck, *PNAS* **2014**, *111*, 63–68.
- [19] J.-F. Ge, Z.-L. Liu, C. Liu, C.-L. Gao, D. Qian, Q.-K. Xue, Y. Liu, J.-F. Jia, *Nat. Mater.* **2015**, *14*, 285–289.
- [20] A. E. Böhmer, F. Hardy, F. Eilers, D. Ernst, P. Adelman, P. Schweiss, T. Wolf, C. Meingast, *Phys. Rev. B* **2013**, *87*.
- [21] Y. Mizuguchi, F. Tomioka, S. Tsuda, T. Yamaguchi, Y. Takano, *Appl. Phys. Lett.* **2008**, *93*, 152505.
- [22] T. Imai, K. Ahilan, F. L. Ning, T. M. McQueen, R. J. Cava, *Phys. Rev. Lett.* **2009**, *102*, 177005.
- [23] S. Medvedev, T. M. McQueen, I. A. Troyan, T. Palasyuk, M. I. Eremets, R. J. Cava, S. Naghavi, F. Casper, V. Ksenofontov, G. Wortmann, C. Felser, *Nat. Mater.* **2009**, *8*, 630–633.
- [24] S. Margadonna, Y. Takabayashi, Y. Ohishi, Y. Mizuguchi, Y. Takano, T. Kagayama, T. Nakagawa, M. Takata, K. Prassides, *Phys. Rev. B* **2009**, *80*, 064506.
- [25] M. Burrard-Lucas, D. G. Free, S. J. Sedlmaier, J. D. Wright, S. J. Cassidy, Y. Hara, A. J. Corkett, T. Lancaster, P. J. Baker, S. J. Blundell, S. J. Clarke, *Nat. Mater.* **2013**, *12*, 15–19.
- [26] S. J. Sedlmaier, S. J. Cassidy, R. G. Morris, M. Drakopoulos, C. Reinhard, S. J. Moorhouse, D. O’Hare, P. Manuel, D. Khalyavin, S. J. Clarke, *J. Am. Chem. Soc.* **2014**, *136*, 630–633.
- [27] M. Bouroushian, *Electrochemistry of Metal Chalcogenides*, of *Monographs in Electrochemistry*, Springer Berlin Heidelberg, Berlin, Heidelberg, **2010**.
- [28] J. Kang, S. A. Wells, V. K. Sangwan, D. Lam, X. Liu, J. Luxa, Z. Sofer, M. C. Hersam, *Adv. Mater.* **2018**, *30*, 1802990.
- [29] P. Marvan, V. Mazánek, Z. Sofer, *Nanoscale* **2019**, *11*, 4310–4317.
- [30] S.-J. Shen, T.-P. Ying, G. Wang, S.-F. Jin, H. Zhang, Z.-P. Lin, X.-L. Chen, *Chinese Phys. B* **2015**, *24*, 117406.
- [31] A. M. Alekseeva, O. A. Drozhzhin, K. A. Dosaev, E. V. Antipov, K. V. Zakharov, O. S. Volkova, D. A. Chareev, A. N. Vasiliev, C. Koz, U. Schwarz, H. Rosner, Y. Grin, *Sci. Rep.* **2016**, *6*, 25624.
- [32] J. R. Dahn, M. A. Py, R. R. Haering, *Can. J. Phys.* **1982**, *60*, 307–313.

- [33] J. N. Reimers, J. R. Dahn, *J. Electrochem. Soc.* **1992**, *139*, 2091–2097.
- [34] M. Kaus, I. Issac, R. Heinzmann, S. Doyle, S. Mangold, H. Hahn, V. S. K. Chakravadhanula, C. Kübel, H. Ehrenberg, S. Indris, *J. Phys. Chem. C* **2014**, *118*, 17279–17290.
- [35] I. Bezza, M. Kaus, L. Riekehr, L. Pfaffmann, S. Doyle, S. Indris, H. Ehrenberg, A. Solhy, I. Saadoune, *Phys. Chem. Chem. Phys.* **2016**, *18*, 10375–10382.
- [36] B. Rasche, H. M. A. Amin, S. J. Clarke, R. G. Compton, *J. Electroanal. Chem.* **2019**, *835*, 239–247.
- [37] G. Hägg, A.-L. Kindström, *Z. Phys. Chem.* **1933**, *22B*, 453–464.
- [38] T. Tsuji, A. T. Howe, N. N. Greenwood, *J. Solid State Chem.* **1976**, *17*, 157–163.

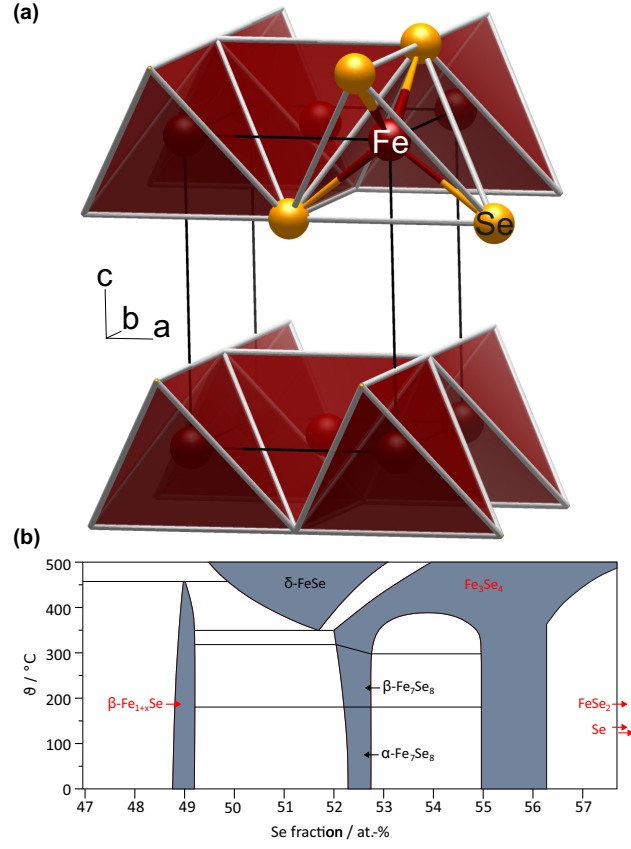


FIG. 1. (a) Unit cell of the  $\beta$ - $\text{Fe}_{1+x}\text{Se}$  structure (anti-PbO type)  
 (b) Fe-Se phase diagram in the vicinity of the 1:1 composition.[9]

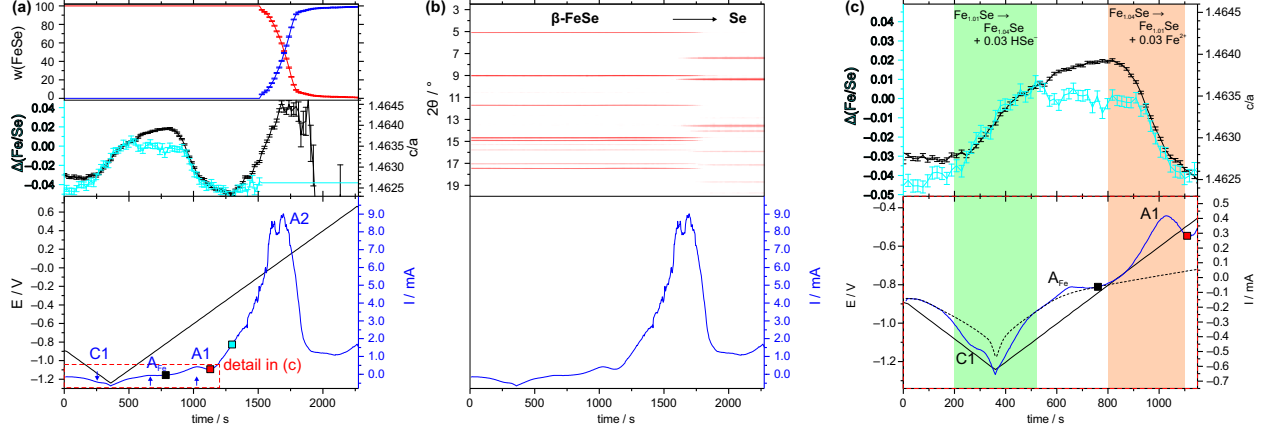


FIG. 2. (a) Linear Sweep Voltammetry (LSV) at  $0.001 \text{ Vs}^{-1}$  with the potential being swept from  $-0.8 \text{ V}$  to  $-1.25 \text{ V}$  and to  $0.7 \text{ V}$  (bottom: black) with the **current response** (bottom: blue; dashed red rectangle see (c)), the mass fraction of  $\beta\text{-Fe}_{1+x}\text{Se}$  (top: red) and **selenium** (top: blue), and the  $\Delta$  (Fe/Se-ratio) (centre: turquoise) and the  $c/a$ -ratio (centre: black). The black, red and turquoise square mark the stages at which samples for the magnetisation measurements were extracted (see text).

(b) Contour plot showing the strongest diffraction peaks and indices in the course of the LSV experiment (X-ray wavelength  $\lambda = 0.494 \text{ \AA}$ ) with the current response from (a) as guideline.

(c) Zoom of the LSV experiment from (a) into the region of the partial oxidation of  $\beta\text{-Fe}_{1+x}\text{Se}$ .



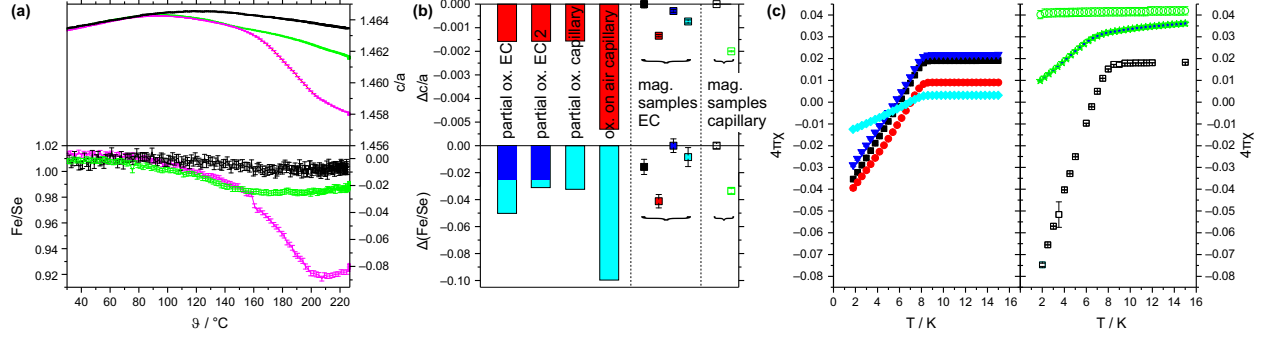


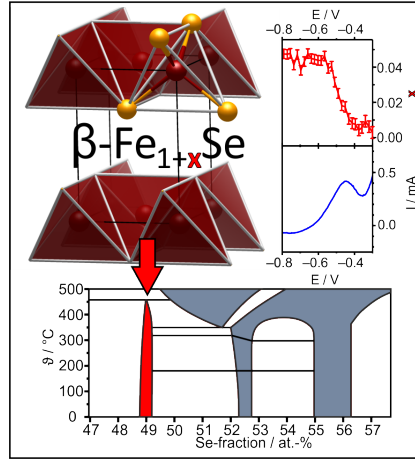
FIG. 3. (a)  $c/a$ -ratio (top) and Fe/Se-ratio (bottom) in  $\beta\text{-Fe}_{1+x}\text{Se}$  from Rietveld refinement during an in-situ diffraction experiment while heating a sample under argon (black), with a fixed amount of oxygen (green) and in air (magenta).

(b) Comparison of the change in the  $c/a$ -ratio (top) and the Fe/Se-ratio (bottom) for the in-situ diffraction samples from the electrochemical oxidation (EC and EC2, see Figure 2b and SI Figure S.9b) and the capillary samples with a fixed amount of oxygen and in air (partially and fully oxidised) and the samples used for magnetisation measurements (same colour code as (c); corresponding to stages shown in Figure 2a and c). Blue corresponds to the change of the Fe/Se-ratio according to the integrated charge (only for EC and EC2).

(c) left: magnetic susceptibility for electrochemically treated samples (zero field cooled): reduced C1 (black), oxidised A1 (red), re-reduced in  $\text{Fe}^{2+}$  solution (blue), oxidised halfway into full oxidation A2 (turquoise). Respective stages shown as squares in Figure 2a and c.

right: magnetic susceptibility for  $\beta\text{-Fe}_{1+x}\text{Se}$  after heating under argon as shown in (a) (black; coincides with curve after synthesis), after the oxidation with a fixed amount of oxygen as in (a) (green) and after electrochemical reduction of the oxidised sample (blue-green stars).

## GRAPHICAL ABSTRACT



Electrochemically accessing the phase width of the superconductor  $\beta\text{-Fe}_{1+x}\text{Se}$  combined with in-situ synchrotron XRD reveals superconductivity for all  $x$ . Oxidation of the same structure under air above 100 °C destroys the superconductivity. The latter can be reinstated by electrochemical reduction.